



THE UNIVERSITY *of* EDINBURGH

Edinburgh Research Explorer

## Tau assemblies do not behave like independently acting prion-like particles in mouse neural tissue

**Citation for published version:**

Miller, L, Mukadam, A, Durrant, C, Vaysburd, M, Katsinelos, T, Tuck, B, Sanford, S, Sheppard, O, Knox, C, Cheng, S, James, L, Coleman, M & McEwan, W 2021, 'Tau assemblies do not behave like independently acting prion-like particles in mouse neural tissue', *Acta Neuropathologica Communications*, vol. 9, no. 41, 41. <https://doi.org/10.1186/s40478-021-01141-6>

**Digital Object Identifier (DOI):**

[10.1186/s40478-021-01141-6](https://doi.org/10.1186/s40478-021-01141-6)

**Link:**

[Link to publication record in Edinburgh Research Explorer](#)

**Document Version:**

Publisher's PDF, also known as Version of record

**Published In:**

Acta Neuropathologica Communications

**General rights**

Copyright for the publications made accessible via the Edinburgh Research Explorer is retained by the author(s) and / or other copyright owners and it is a condition of accessing these publications that users recognise and abide by the legal requirements associated with these rights.

**Take down policy**

The University of Edinburgh has made every reasonable effort to ensure that Edinburgh Research Explorer content complies with UK legislation. If you believe that the public display of this file breaches copyright please contact [openaccess@ed.ac.uk](mailto:openaccess@ed.ac.uk) providing details, and we will remove access to the work immediately and investigate your claim.

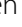


RESEARCH

Open Access



# Tau assemblies do not behave like independently acting prion-like particles in mouse neural tissue

Lauren V. C. Miller<sup>1†</sup> , Amir S. Mukadam<sup>1†</sup>, Claire S. Durrant<sup>2,4</sup>, Marina J. Vaysburd<sup>3</sup>, Taxiarchis Katsinelos<sup>1</sup>, Benjamin J. Tuck<sup>1</sup>, Sophie Sanford<sup>1</sup>, Olivia Sheppard<sup>2</sup>, Claire Knox<sup>3</sup>, Shi Cheng<sup>1</sup>, Leo C. James<sup>3</sup>, Michael P. Coleman<sup>2</sup> and William A. McEwan<sup>1\*</sup>

## Abstract

A fundamental property of infectious agents is their particulate nature: infectivity arises from independently-acting particles rather than as a result of collective action. Assemblies of the protein tau can exhibit seeding behaviour, potentially underlying the apparent spread of tau aggregation in many neurodegenerative diseases. Here we ask whether tau assemblies share with classical pathogens the characteristic of particulate behaviour. We used organotypic hippocampal slice cultures from P301S tau transgenic mice in order to precisely control the concentration of extracellular tau assemblies in neural tissue. Whilst untreated slices displayed no overt signs of pathology, exposure to recombinant tau assemblies could result in the formation of intraneuronal, hyperphosphorylated tau structures. However, seeding ability of tau assemblies did not titrate in a one-hit manner in neural tissue. The results suggest that seeding behaviour of tau arises at high concentrations, with implications for the interpretation of high-dose intracranial challenge experiments and the possible contribution of seeded aggregation to human disease.

**Keywords:** Prion-like activity, Tau seeded aggregation, Organotypic hippocampal slice cultures, Neurodegeneration, Tauopathies

## Introduction

Neurodegenerative diseases are typified by the accumulation of specific proteins into fibrillar assemblies. In around twenty distinct neurodegenerative diseases, including the most common, Alzheimer's disease, the protein tau forms hyperphosphorylated, filamentous inclusions within the cytoplasm of neurons. Tau pathology can be a direct cause of neurodegeneration. For instance, human genetic studies reveal that around 50 distinct mutations in *MAPT*, the gene that encodes tau,

cause inherited forms of dementia with evidence of tau filaments [1]. The origin of tau assemblies in the human brain remains uncertain. Cell-autonomous processes may lead to the spontaneous nucleation of oligomeric forms of tau within the cytoplasm of neurons. Some of these assemblies adopt filamentous conformations that are able to undergo extension by the addition of tau monomers to the filament ends. Over the past decade it has been postulated that, in addition to these cell-autonomous mechanisms, tau pathology may occur through a spreading or 'prion-like' mechanism [2]. Several lines of evidence demonstrate that assemblies of tau can be taken up into cells, whereupon they seed the conversion of native tau to the assembled state. Addition of tau assemblies to the exterior of cells, or the injection of tau assemblies

\*Correspondence: wm305@cam.ac.uk

<sup>†</sup>Lauren V. C. Miller and Amir S. Mukadam have contributed equally to this work.

<sup>1</sup> Department of Clinical Neurosciences, UK Dementia Research Institute at the University of Cambridge, Cambridge, UK

Full list of author information is available at the end of the article



into the brains of tau-transgenic and wildtype mice, can induce intracellular tau assembly in the recipient [3–6].

Population cross-sectional studies demonstrate that the appearance of tau pathology follows a predictable pattern over time and space in the human brain, potentially indicating spreading via a prion-like mechanism. Immunoreactivity to antibodies such as AT8, which detects tau that is phosphorylated at positions S202 and T205 [7], progresses in a manner that can be systematically categorised into stages according to anatomical distribution (Braak stages 0–VI) [8, 9]. In young adults, some AT8 immunoreactivity is observed in the vast majority of brains by the third decade of life. However, it is generally confined to neurons within the locus coeruleus (LC) in the brainstem (Braak pretangle stages 0 a–c and 1a,b). Subsequently, AT8 staining is observed in the entorhinal cortex (EC) and hippocampus (HC) (Braak stages I–II). Later stages are characterised by progressive dissemination and increasing density of staining in neocortical regions (Braak stages III–VI). These late stages are associated with severe disease and the overall burden of tau pathology negatively correlates with cognitive function [10].

Though intracranial challenge experiments demonstrate that seeded aggregation can in principle occur, they provide little insight as to whether physiological concentrations of extracellular tau species might support prion-like activity. The concentration of tau in wildtype mouse interstitial fluid (ISF) is around 50 ng/ml total tau (equivalent to ~1 nM tau monomer). Wildtype mouse ISF levels typically exceed cerebrospinal fluid (CSF) tau levels by around tenfold [11]. In humans between ages 21–50 years, CSF total tau is below 300 pg/ml increasing to 500 pg/ml over age 70 [12]—approximately 7–12 pM if considering the average mass of full length tau isoforms. Levels are increased 2–threefold in Alzheimer’s disease [13]. If a similar relationship between ISF and CSF tau concentration exists in humans as in mice, ISF tau levels are likely in the order of 100 pM, rising to 300 pM in Alzheimer’s disease. Intracranial injection experiments typically supply tau in the high micromolar range. Even if this were distributed broadly across the brain, micromolar concentrations would be exceeded and local concentration at the injection site may plausibly be 100-fold greater. Thus, intracranial injection experiments likely exceed physiological concentrations of extracellular tau by two to seven orders of magnitude.

For classical infectious agents, infectivity is related to dose by a “one-hit” relationship wherein the amount of infectivity decreases linearly upon dilution until endpoint [14]. This property is also evident in PrP<sup>Sc</sup> prions, though it is complicated by the presence of multiple aggregation states and the size distribution of particles

[15]. The relationship between dose and prion-like activity for tau has not been established. It is therefore currently not possible to reconcile high-dose challenge experiments with the low concentrations of tau observed in the extracellular spaces of the brain. To address this, we developed a model of seeded tau aggregation in mouse organotypic hippocampal slice cultures, allowing direct control of the concentration of tau neurons were exposed to. Brain slice cultures have been used for over 40 years [16], though developments in recent years have rendered them increasingly relevant for the study of neurodegenerative diseases [17–21]. We prepared slices from transgenic mice expressing human tau bearing the P301S mutation [22], which is causative of familial frontotemporal dementia and displays accelerated fibrilisation compared to wildtype tau [23].

Using our system, we show that neurons within CA1 are preferentially susceptible to seeded aggregation, displaying intracellular hyperphosphorylated tau tangles. We find that seeding activity cannot be titrated down and only occurs at high concentrations of tau assemblies. The concentrations of tau assemblies required to initiate seeding in this model exceed reported physiological ranges of ISF and CSF tau. Our results imply that a model of tau spread via seeded aggregation requires these concentrations to be locally exceeded or requires other mechanisms not captured here to facilitate seeded aggregation.

## Results

Sagittal hippocampal slices of ~300 µm thickness were prepared from homozygous P301S tau-transgenic mice at age 7 d, and cultured at the air–liquid interface on culture support membranes (Fig. 1a). Hippocampal structures are well developed at this age, yet the tissue exhibits plasticity that aids recovery from the slicing procedure [24]. We stained OHSCs with antibodies against markers of the major cell types of the brain: neurons (Map2), microglia (Iba1) and astrocytes (Gfap) (Fig. 1b). Similar to previous studies [20], neurons were found to maintain extensive arborisation with evidence of intact neuronal tracts. Microglia were observed with normal morphology with extensive processes, similar to quiescent cells in whole brains [25]. Astrocytes were also well represented throughout the cultures. Immunostaining for P301S tau revealed widespread expression in all regions of the hippocampus (Fig. 1c). After 5 weeks in culture no overt signs of tau pathology were apparent, as visualised by staining with AT8 (Fig. 1d). These results demonstrate that hippocampal architecture and cell types from P301S tau transgenic mice are maintained through the slicing and culture process. Importantly, they demonstrate that OHSCs from P301S tau transgenic mice do not undergo

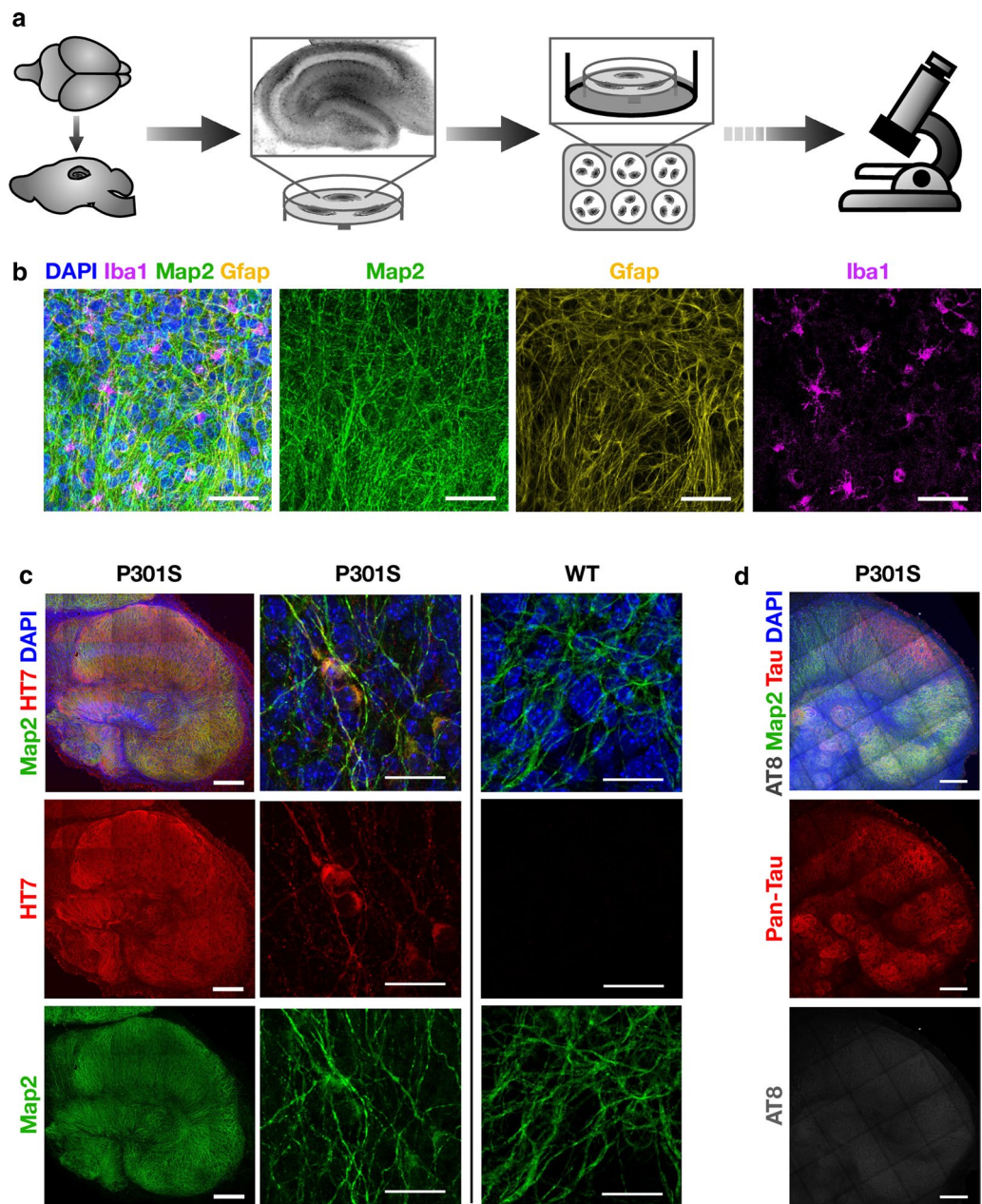
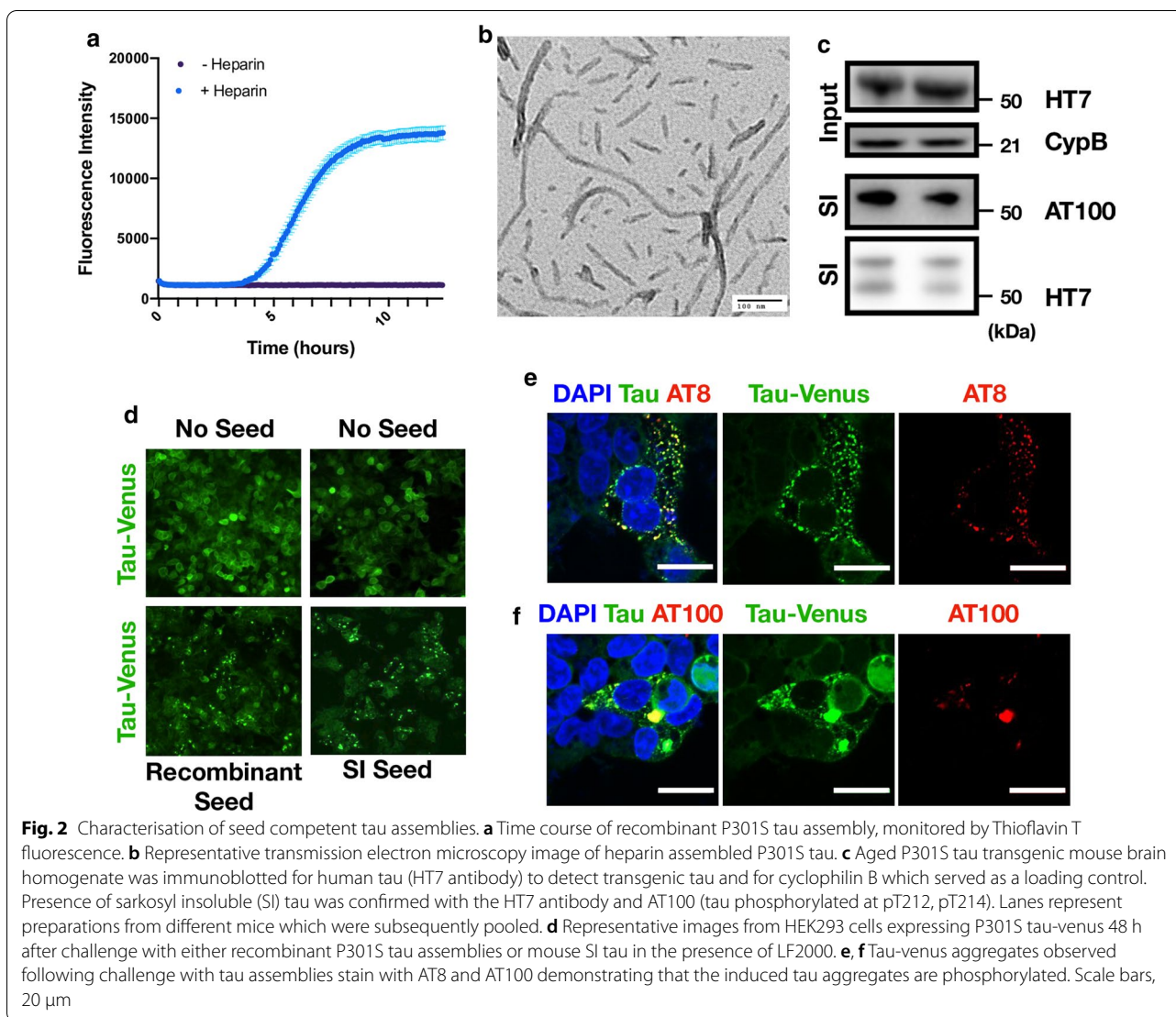


**Fig. 1** Organotypic hippocampal slice cultures (OHSCs) maintain cellular diversity and display no spontaneous tau pathology. **a** Schematic of the production of OHSCs. 300 μm thick sagittal slices are cut from brain hemispheres. The hippocampus is then dissected and cultured at the air-liquid interface on semi-permeable membranes with media supplied to the basal side of the membrane. **b** OHSCs from mice transgenic for P301S tau were fixed after 2 weeks in culture and stained for nuclei (DAPI), the neuronal marker Map2, the astrocyte marker Gfap, and the microglial marker Iba1. Scale bars, 50 μm. **c** OHSCs from P301S tau transgenic mice stain positive for human tau-specific antibody HT7 whereas OHSCs from WT mice do not. Scale bars, 250 μm and 25 μm. **d** OHSCs from P301S tau transgenic mice after 5 weeks in culture display only background levels of staining with the phospho-tau specific antibody AT8. Slices were stained with DAPI and Map2 as above and with pan-tau. Scale bars, 250 μm

detectable spontaneous aggregation over this time period.

To investigate the response of slice cultures to challenge with tau assemblies, we prepared tau from two independent sources. First, we expressed the ON4R

isoform of tau bearing the P301S mutation in *E. coli*. Recombinant protein was incubated with heparin and, following a lag period, was found to give a fluorescent signal in the presence of thioflavin T, a dye whose fluorescence increases upon binding to β-sheet rich amyloid



structures (Fig. 2a). Negative stain transmission electron microscopy revealed the presence of abundant filamentous structures (Fig. 2b). Second, we prepared the sarkosyl-insoluble (SI) fraction from aged P301S tau transgenic mice, a procedure that enriches insoluble tau species. Brain-derived assemblies were subjected to western blot, confirming the presence of hyperphosphorylated, insoluble tau (Fig. 2c). The samples were quantified using a dot-blot method using recombinant fibrillar tau as a standard (Additional file 1: Supplementary Fig. 1). Tau assemblies were added to HEK293 cells stably expressing 0N4R P301S tau-venus, a reporter cell line for seeded aggregation [26]. In this assay, transfection reagents are used to deliver tau assemblies into cells, whereupon tau-venus is observed to form puncta over 1–2 d. This aggregation was previously found to result in the accumulation of tau-venus in the sarkosyl-insoluble pellet [26]. In the

present study, abundant venus-positive puncta were detected following challenge with recombinant fibrils or mouse brain derived tau (Fig. 2d). To investigate whether these seeded assemblies bore markers of tau hyperphosphorylation, we stained with the monoclonal antibody AT8 and AT100, which recognises tau phosphorylated at pT212 and pS214. These epitopes occur on tau filaments extracted from post-mortem tauopathy brains, including those from Alzheimer’s disease patients. We observed that challenge with recombinant tau assemblies resulted in colocalization between tau-venus puncta and AT8 or AT100 (Fig. 2e, f). We therefore concluded that our tau preparations contained species able to induce *bona fide* seeded aggregation in recipient cells.

To test whether OHSCs support seeded aggregation, we treated slices at DIV7 with recombinant tau assemblies or mouse brain derived sarkosyl insoluble (SI) tau.

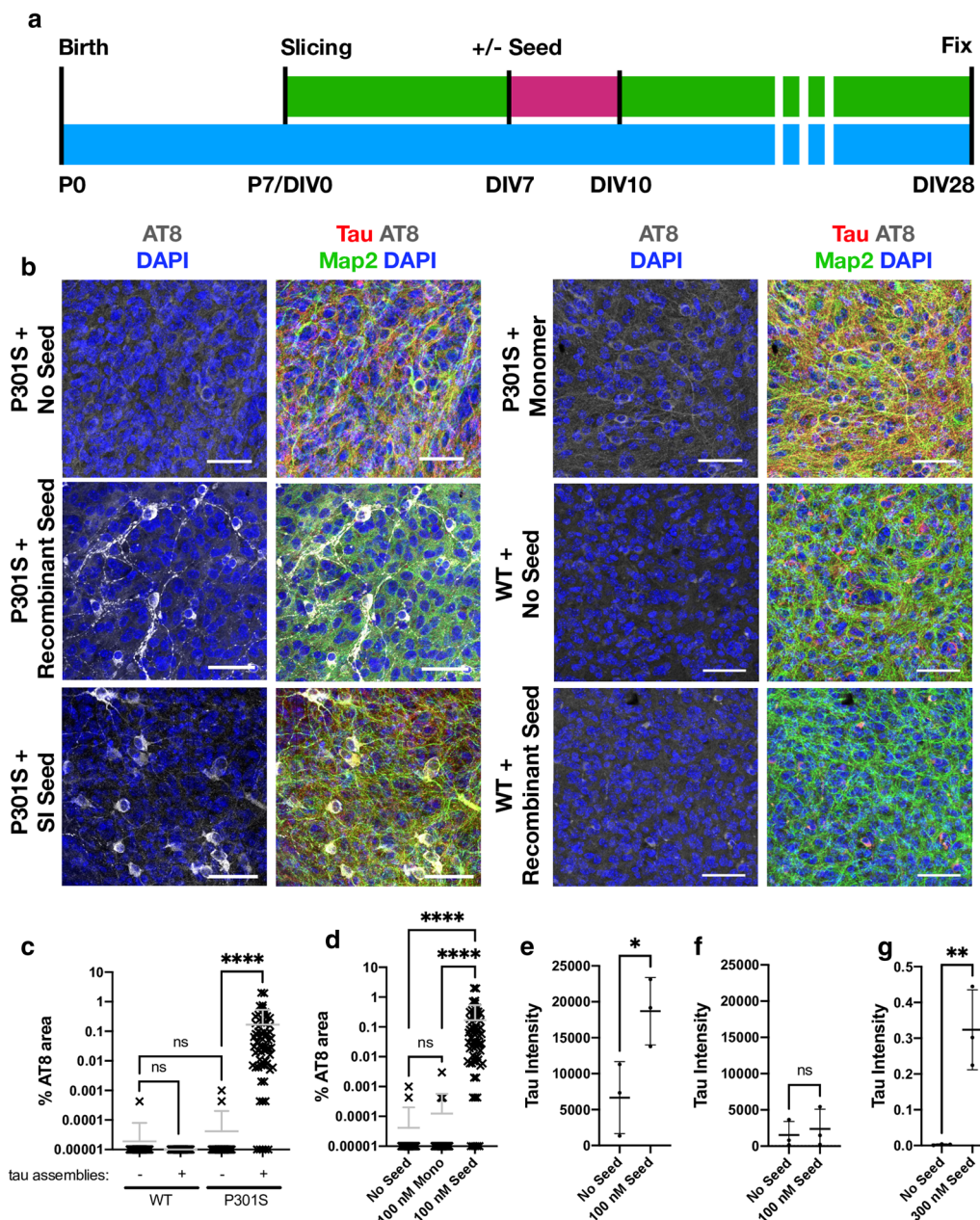


**Fig. 3** Challenging OHSCs with exogenous tau assemblies induces seeded tau aggregation. **a** Timeline of organotypic hippocampal slice culture preparation and treatment. OHSCs were prepared from P7 pups. After 7 days in vitro (DIV), tau assemblies were added to the media and incubated for 3 days. A complete media change was carried out at the end of the seeding period (pink). At other times (green) 50% media changes were performed twice weekly until fixation at 28 days in vitro (DIV). **b** OHSCs derived from P301S tau transgenic mice were challenged with either 100 nM recombinant tau assemblies, 100 nM monomeric tau, 5  $\mu$ L (~300 nM) of mouse brain origin sarkosyl insoluble (SI) tau or buffer only. WT OHSCs were challenged with 100 nM recombinant tau assemblies or buffer only. Scale bars, 50  $\mu$ m. **c** Quantification of seeding levels in WT and P301S tau transgenic OHSCs, following addition of 100 nM recombinant tau assemblies or buffer only. **d** Levels of AT8 immunostaining following challenge of OHSCs with monomeric tau (Mono) or heparin assembled tau (Seed). **e, f** Levels of sarkosyl insoluble tau present in transgenic P301S (e) or WT (f) OHSCs with and without the addition of 100 nM recombinant tau assemblies. Data derived from Western blot, normalised to input levels of tau and loading control. **g** Levels of human tau (HT7) present in WT OHSCs after 3 days of exposure to 300 nM recombinant tau assemblies applied beneath the membrane. **c** and **d**, statistical significance determined by Kruskal–Wallis test by ranks and Dunn’s multiple comparisons test. **e–g** statistical significance determined by unpaired t-test. For panels **c–f**, data points represent individual fields of view from multiple slices derived from N = 3 mice per condition. \*\*\*\* $P < 0.0001$ ; \*\* $P < 0.01$ ; \* $P < 0.05$ ; ns, not significant)

After three days a complete media change was performed to remove the tau, and the OHSCs were incubated for a further three weeks (Fig. 3a). Following treatment with tau assemblies, we observed pronounced AT8 staining, suggesting the presence of intracellular hyperphosphorylated tau structures (Fig. 3b, c). The addition of monomeric tau did not induce these same structures, indicating that the misfolded state of tau was responsible for seeded aggregation (Fig. 3b, d). Furthermore, addition of tau assemblies to OHSCs prepared from wildtype mice did not induce seeded aggregation suggesting that the transgenic P301S tau construct is responsible for the phenotype (Fig. 3b, c). The hyperphosphorylation of tau was accompanied by the accumulation of sarkosyl-insoluble species following seeding in P301S transgenic OHSCs but not in wildtype OHSCs (Fig. 3e, f) (Additional file 1: Supplementary Fig. 2). Whilst the human transgenic tau is therefore required for seeding to occur, we cannot exclude the possibility that endogenous mouse tau also contributes to aggregates in the transgenic slices since the AT8 epitope is identical between human and mouse tau. To test whether exogenously applied tau could be found within the slices, recombinant tau assemblies were supplied to the culture media of wildtype slices, beneath the membrane, for a period of three days. After this time, we observed human tau present in the slices by western blot, indicating the transfer of tau assemblies from the media to the slice (Fig. 3g) (Additional file 1: Supplementary Fig. 2). Taken together, these data demonstrate that exogenously supplied tau assemblies are taken up into OHSCs and can induce the formation of hyperphosphorylated, insoluble tau species.

To further characterise the induced aggregates, we investigated the subcellular and regional location of tau lesions. We used recombinant tau assemblies to induce seeding owing to the high confidence that AT8-reactive aggregates result from seeded aggregation rather than the input tau. Within cell bodies, we observed large aggregates in peri-nuclear regions (Fig. 4a). Additionally, numerous smaller tau puncta were found along the length of neurites. Puncta were interrupted by regions apparently devoid of hyperphosphorylated tau. In contrast, Map2 staining revealed the presence of intact neurites, indicating that the punctate distribution of tau is not a consequence of neuronal fragmentation. They further demonstrate that neurons are able to tolerate tau aggregation to a certain degree without gross loss of morphology or overt toxicity. We compared levels of seeding between regions of the hippocampal slices. We observed the presence of AT8 positive structures in neurons within all subdivisions (Fig. 4b). However, AT8 reactivity was considerably greater within the CA1 region compared to CA2 and CA3. Approximately 80% of AT8-positive

structures were found in CA1, compared to ~10% in each of CA2 and CA3 (Fig. 4c). We examined levels of tau as a potential underlying cause of CA1 susceptibility but observed comparable expression levels across different regions (Fig. 4d). In summary, these results demonstrate that challenge of OHSCs with assemblies of tau induces the accumulation of pathology in neurites and cell bodies, predominantly in CA1 neurons, resulting in widespread accumulation of intracellular hyperphosphorylated tau structures.

To determine the time-dependence of this tau pathology, we next performed a time course following the addition of seed. Slices were fixed at various time points following challenge with 100 nM recombinant assemblies or buffer only (Fig. 5a). As above, slices that were not exposed to tau assemblies developed no robust evidence of hyperphosphorylated tau puncta. However, challenge with tau assemblies resulted in increasing levels of bright AT8-positive structures over time, consistent with seeded aggregation of intracellular pools of tau (Fig. 5b). At 1 week after challenge, isolated AT8 positive puncta were observed as well as diffuse AT8 staining. A week later, puncta became more numerous and a few large aggregates were observed. At 3 weeks after challenge with tau assemblies, AT8 staining was widespread with the presence of numerous aggregates that occupied entire cell bodies. This level of staining was maintained at approximately the same level between 3 and 4 weeks, suggesting that the induced aggregation is complete at 3 weeks post-challenge in this system. This timepoint was therefore selected for all further experiments. During the first three weeks, AT8 staining followed an exponential curve with a doubling time of just under a week (Fig. 5c). The size of AT8-positive structures was similarly found to increase over time. Stained areas greater than 50  $\mu\text{m}^2$ , generally only present within cell bodies, were found to be largely absent at 1 week post-challenge, but subsequently increased in prevalence (Fig. 5d). This suggests that the amplification of aggregates within individual neurons contributes to the overall increase in AT8 signal. The results are therefore consistent with a model of growth of hyperphosphorylated tau structures via a process of templated aggregation following exposure to seed-competent tau assemblies.

The above results demonstrate that our OHSC model exhibits behaviour consistent with the prion-like spread of tau. However, the dose we used (100 nM monomer equivalent) represents a concentration in excess of ISF and CSF tau concentrations, which occupy the low nanomolar to picomolar region. We therefore investigated the response of OHSCs to varying doses of exogenously supplied tau assemblies. Remarkably, we found that a reduction of seed concentration from 100 to

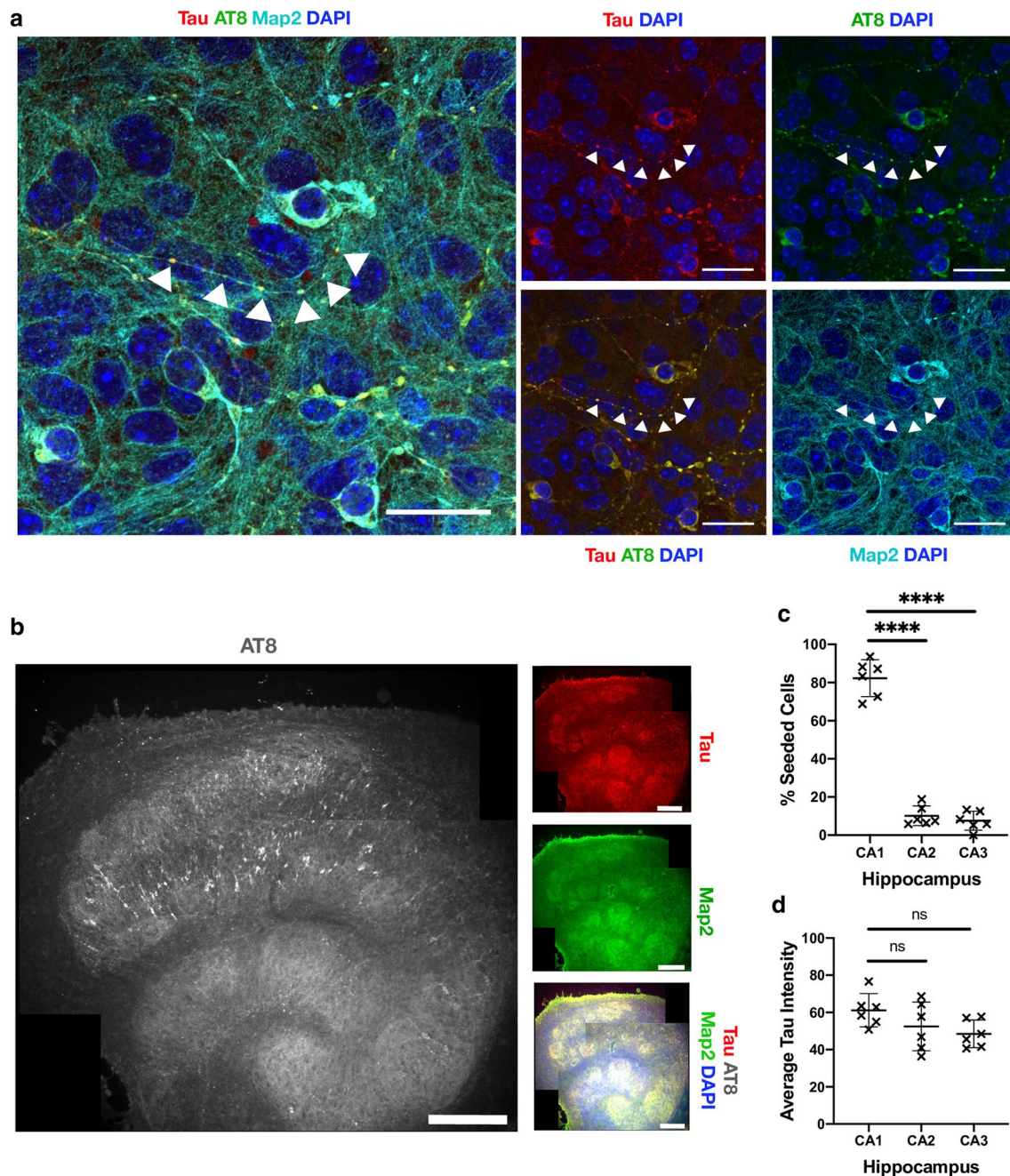


**Fig. 4** Seeded neurons localise to CA1 and display phospho-tau aggregates within intact nerve processes. **a** OHSCs were challenged with 100 nM recombinant tau assemblies to induce seeded aggregation. Hyperphosphorylated tau puncta can be observed along intact nerve processes (arrows) and within cell bodies. Scale bars, 25  $\mu$ m. **b** Tiled image of representative OHSC challenged with 100 nM recombinant tau assemblies displays AT8 immunoreactivity predominantly in the CA1 subregion. Scale bars, 250  $\mu$ m. **c** The distribution of seeded cells in hippocampal subregions was quantified by counting cells positive for AT8 aggregates. **d** Levels of tau, as quantified by immunofluorescence staining with pan-tau antibody, shows that CA1, CA2 and CA3 express similar levels of tau. Statistical significance for c and d determined by one-way ANOVA and Tukey's post hoc multiple comparisons test (multiple fields imaged from N = 6 mice. \*\*\*\* $P < 0.0001$ )

30 nM resulted in virtually no seeded aggregation being detectable within the slice at three weeks post-challenge (Fig. 6a). Whereas cell bodies reactive for AT8 could be

observed when challenged with 100 nM tau assemblies, only very rare and small AT8-positive assemblies in neurites were observed following challenge with 30 nM tau.



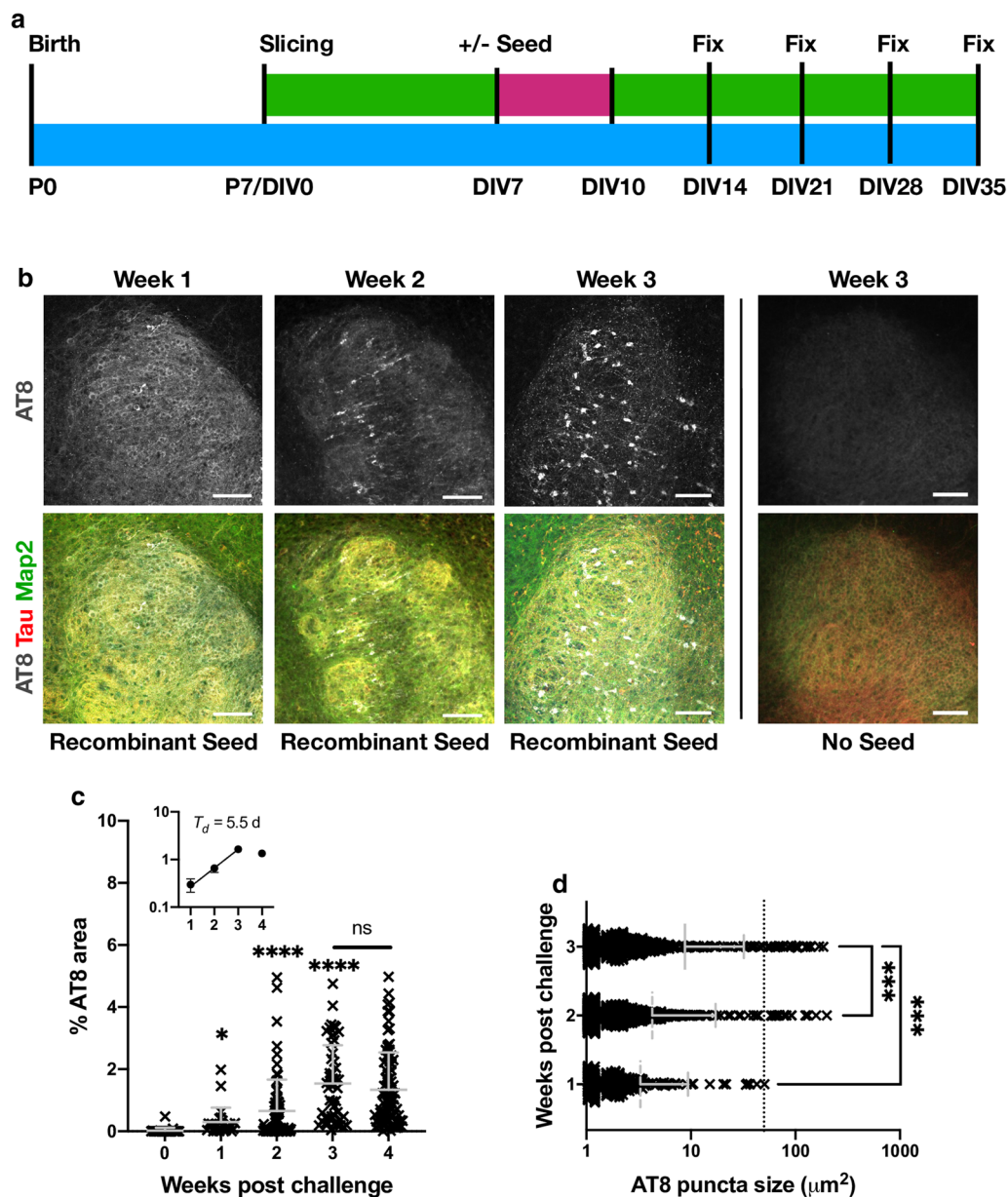
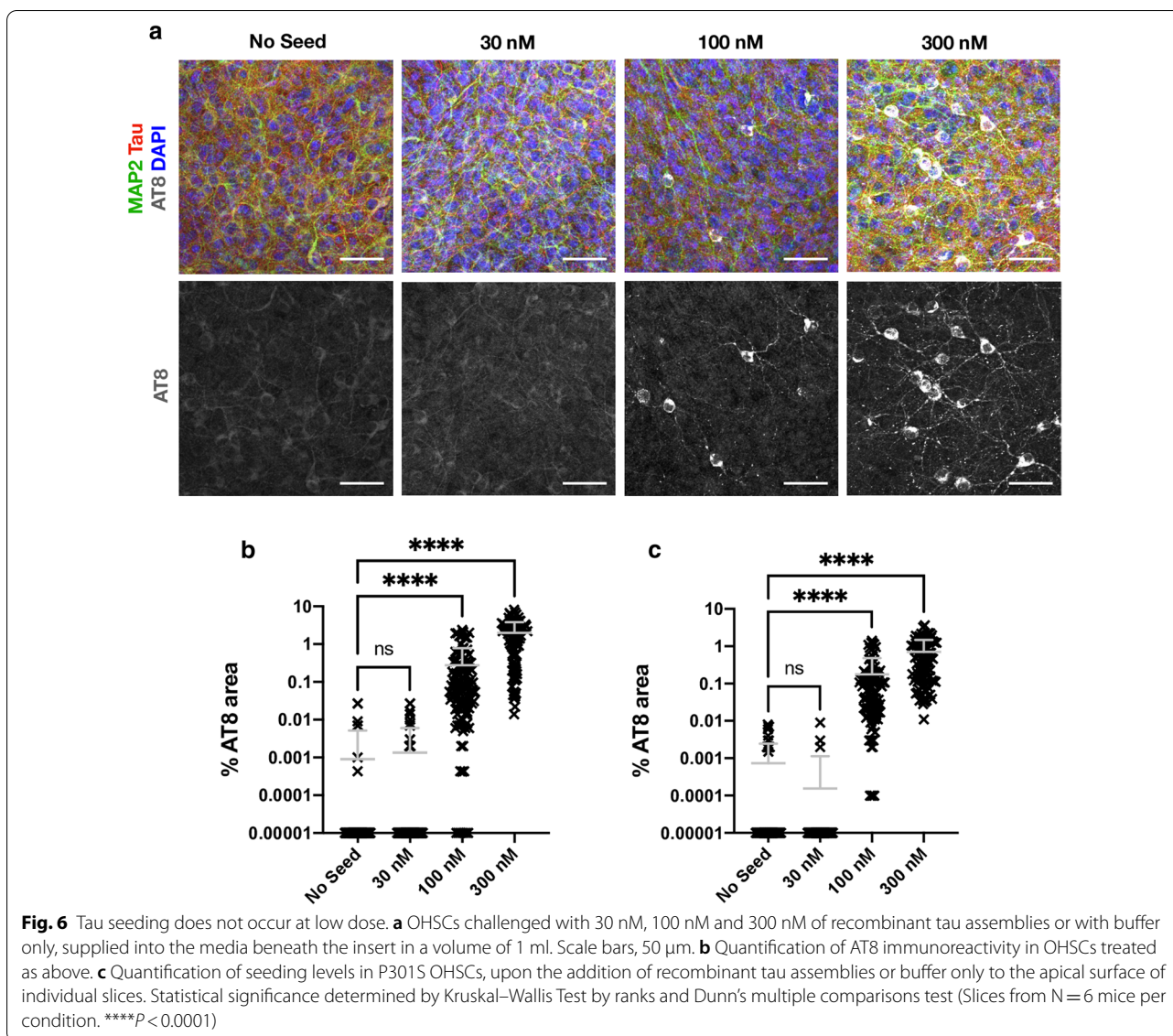


**Fig. 5** Seeded aggregation occurs over three weeks. **a** Schematic of OHSC treatment. 100 nM recombinant tau assemblies were added to the media as previous and left for 3 days (pink) followed by a complete media change. Subsequently 50% media changes were performed twice weekly (green) until fixation at 1, 2, 3 or 4 weeks post challenge. **b** Slices fixed at 1 week post challenge display diffuse AT8 staining. Slices fixed at 2 or 3 weeks demonstrate increasing levels of AT8 reactivity in cell bodies and neurites. OHSCs not challenged with exogenous tau assemblies exhibit only diffuse background levels of AT8 reactivity. Scale bars, 100  $\mu\text{m}$ . **c** Percent AT8-positive area increases over time following challenge with recombinant tau assemblies. Statistical significance determined by Kruskal–Wallis Test by ranks and Dunn’s multiple comparisons test compared to 0 weeks post challenge unless indicated (multiple fields imaged from slices from  $N=3$  mice, per time point. \* $P<0.05$ , \*\*\*\* $P<0.0001$ ). Inset represents the same data from weeks 1–4 plotted on a logarithmic scale. Doubling time ( $T_d$ ) estimated from linear regression curve fitted to data up to 3 weeks. **d** AT8 positive puncta increase in size following challenge with 100 nM recombinant assemblies. Dotted line at  $50 \mu\text{m}^2$  represents approximate lower size limit of cell body-occupying lesions. Statistical significance determined by Kruskal–Wallis Test by ranks and Dunn’s multiple comparisons test (multiple fields imaged from slices from  $N=3$  mice at each time point. \*\*\* $P<0.001$ )

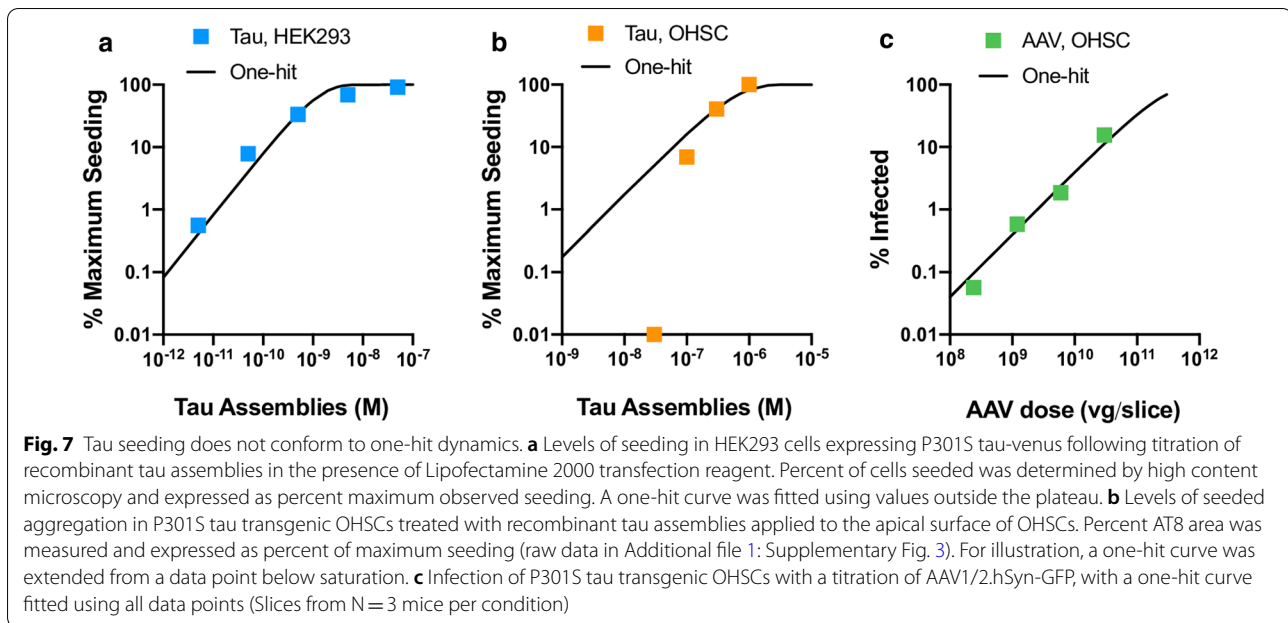
Conversely, increasing exogenous tau concentration from 100 to 300 nM increased the AT8-immunoreactive area by almost tenfold, consistent with a non-linear effect

of tau concentration in this range (Fig. 6b). To exclude any effect of the culture membrane on the efficiency of tau uptake, we applied tau at the same concentrations



directly to the apical surface of the slices in a volume of 20  $\mu$ l. Under both experimental set-ups we observed robust induction of seeding at 100 nM, but not at 30 nM (Fig. 6c). Thus, the local concentration of tau governs seeded aggregation and is independent of application route. The smaller volumes required for apical application of tau permitted challenge with an extreme concentration of supplied tau, at 1000 nM. Here we observed a plateauing of percent AT8-positive area and the presence of AT8 reactivity in almost all neurons (Additional file 1: Supplementary Fig. 3). These results demonstrate that tau seeding in OHSCs only occurs efficiently at concentrations above 100 nM of supplied assemblies, and plateaus in the low micromolar range.

Independently acting infectious particles such as viruses retain infectivity upon dilution until they are diluted out at endpoint. They display one-hit dynamics where the proportion of infected cells,  $P(I)$ , can be described by the equation  $P(I) = 1 - e^{-m}$  where  $m$  is the average number of infectious agents added per cell. To determine whether tau assemblies display these properties, we titrated tau assemblies onto HEK293 cells expressing P301S tau-venus. Here, where conditions have been optimised for sensitive detection of seeding, and tau assemblies are delivered directly to the cytoplasm with transfection reagents, we observe that seeding activity is proportional to dose and can be titrated down. The observed level of seeding closely follows a one-hit titration curve (Fig. 7a). Thus, tau assemblies have the



intrinsic ability to act as independent particles when tested in reporter cell lines. This is in direct contrast to the results observed in OHSCs where seeding reduces much more rapidly as tau assemblies are diluted than would be expected under a single-hit model (Fig. 7b). One potential explanation for these differences is that clearance mechanisms in intact tissue inherently prevent single-particle activity. To test this, we titrated AAV1/2.hSyn-GFP particles expressing GFP and measured the percent of Map2-positive neurons that were transduced. We observed that AAV1/2 behaved in a manner consistent with one-hit dynamics (Fig. 7c). Thus, tau assemblies differ from classical infectious agents and do not titrate in a manner expected of independently acting particles in mouse neural tissue. Rather, in this system, seeding is a behaviour that only emerges at high concentrations of extracellular tau assemblies.

## Discussion

### Study summary

Elucidating the mechanism of tau aggregation and its apparent spread through the brain is critical to the development of mechanism-based therapeutics. The ‘prion-like’ model of tau spread posits that the transit of assembled tau species from affected to naïve cells promotes the exponential spread of pathological tau over time within a diseased brain. In support of this model, extracellular fluids of tauopathy patients’ brains contain seed-competent tau species: CSF samples from both AD and Pick’s disease patients give rise to seeded aggregation in biosensor cell lines and biochemical detection assays

[27–29]. Further evidence in support of the prion-like model comes from in vivo challenge experiments: intracranial injection of assembled tau can result in induced tau pathology in wildtype or tau-transgenic rodent brains. Understanding whether the behaviour of tau is conserved between the high concentrations typically used in in vivo injection experiments, and the low levels present in the extracellular spaces of the brain, is important when assessing the possible contribution of seeded aggregation as a disease mechanism.

To investigate the dose–response of tau assemblies in neural tissue, we established an organotypic hippocampal slice culture system for studying seeded aggregation that, unlike whole animal studies, allows precise control of tau assembly concentration and exposure time. We prepared recombinant tau assemblies with confirmed seeding activity and applied these assemblies to OHSCs from P301S tau transgenic mice. We observed that tau pathology in the OHSCs increased over a period of three weeks, at which point cell body-occupying, hyperphosphorylated tau lesions were observed. This was associated with the accumulation of tau in the sarkosyl insoluble fraction. No overt signs of cell death were observed, and neurons bearing tau lesions with intact processes were evident. Seeded aggregation was dependent on transgenic human tau, since no seeded aggregation was observed in wildtype mouse OHSCs. While others have reported seeded aggregation of wildtype murine tau following challenge with human brain-origin tau assemblies [6], we consider it likely that the P301S tau assemblies preferentially seed the homotypic P301S tau within the neurons.

Surprisingly, we found that tau seeding activity rapidly dropped away upon dilution in OHSCs. Dilution of tau assemblies to 30 nM or below prevented essentially all seeded aggregation. This concentration is long before end-point dilution of tau assemblies and represents a marked deviation from one-hit dynamics. In contrast, tau assemblies displayed one-hit dynamics when delivered directly to the cytoplasm in a HEK293 cell line modified to express P301S tau-venus.

Deviations from one-hit dynamics in virus infection can be caused by host cell factors that prevent infection at low viral dose, but become saturated at high viral dose [30, 31]. By analogy, we consider it likely that homeostatic mechanisms act to prevent seeded aggregation of tau but become saturated by high tau concentrations. The nature of any such saturable barrier to seeding is not clear. One possibility is that phagocytic cells present in slices preclude observations of one-hit dynamics. However, AAV particles were found to titrate with one-hit dynamics in OHSCs, demonstrating one-hit dynamics can be observed in neurons in the presence of glia. A trivial explanation of tau at low concentrations being unable to cross the culture support membrane was also ruled out by also applying tau to the apical side of the OHSCs. Here, we observed the same dynamics, with loss of seeding activity at 30 nM. Other mechanisms are therefore implicated such as saturation of proteostatic mechanisms or saturation of cellular uptake pathways. Identification of these defences may provide a valuable route to understanding the homeostatic mechanisms which prevent the prion-like propagation of tau, and their potential deterioration in disease.

#### Limits of this study

There are certain caveats and limitations of our model that require examination before considering the results in the context of disease. First, the tau species present in the extracellular spaces of the brain are likely to differ from those used here. We have used heparin-assembled recombinant filaments, which are known to differ in structure from brain-derived filaments [32]. Second, brain-origin fibrils have extensive post-translational modifications including hyperphosphorylation and proteolytic truncation, which may alter activity compared to the full-length tau isoform used here that lacks phosphorylation. Though the effects that fibril structure and post-translational modifications have on biological activity are poorly defined, we cannot exclude that brain-origin assemblies retain seeding potency at lower concentrations. Finally, we have used a transgenic animal that expresses P301S human tau as a model of tau pathology. Given that P301S is a pro-aggregant mutation that undergoes enhanced fibrilisation [23] compared to

wildtype tau it would be expected that the transgenic tau would be more sensitive to seeded aggregation. However, there may be unexpected effects in wildtype systems not captured here. Additionally, the endogenous mouse tau may have further effects on the phenotype we observe in the P301S OHSCs. For instance, it has previously been shown that endogenous mouse tau can partially inhibit transgene aggregation [33]. Further research is therefore required to determine whether the loss of seeding potency at low concentrations is a general feature of tau assemblies in neural tissue.

#### Implications of the results

Notwithstanding the caveats above, our results suggest that healthy neural tissue is able to withstand the concentration of tau present in extracellular fluids without observable seeded aggregation. The effective threshold for seeding, measured here at around 100 nM, exceeds physiological ISF/CSF concentrations by several orders of magnitude. Thus, the results suggest that other mechanisms are required in order for seeded aggregation to occur in the brain. For instance, uncontrolled neuronal cell death or release of tau into synaptic clefts may transiently raise the local concentration of tau to high levels. Alternatively, the threshold for seeded tau aggregation may be altered in the degenerating brain, for instance through inflammation or other mechanisms. Finally, other modes of transmission within the brain that do not rely on naked pools of extracellular tau may circumvent the non-linear dose response observed here. Such mechanisms include tau spreading via tunnelling nanotubules and in extracellular vesicles [34, 35].

One of the main pieces of evidence in support of the 'prion-like' hypothesis of tau spread in human disease is the induction of seeded aggregation in mouse neurons following intracranial injection of tau assemblies. These studies have been performed in multiple mouse models, with various ages of animal and with multiple sources of tau assemblies (Additional file 1: Supplementary Table 1). However, the doses injected are mostly in the tens of micromolar range, thus exceeding physiological ISF/CSF tau concentrations by several orders of magnitude. Diffusion after injection is likely to reduce the effective concentration that neurons are exposed to, though for many of these experiments, levels are still likely to exceed micromolar concentrations even if diluted across the whole brain. The data we present here suggests that these experiments may not be simply extrapolated downwards to infer the behaviour of tau assemblies at low concentrations. Rather, our results imply that seeding activity is an emergent property of high doses of tau assemblies when applied extracellularly to neural tissue.

It is not usually clear from studies available in the literature if lower doses were attempted but failed to support seeded aggregation, or if higher doses were selected for other practical purposes. Potentially of interest in this regard is the study by Skachokova and colleagues who successfully induced seeding following injection of P301S tau transgenic mice with a 1000-fold concentrate of CSF from AD patients [36]. At 4–17 nM, these samples are still far in excess of human CSF tau concentrations. But, notably, these concentrations are below the threshold defined in our OHSC model, signifying different tau preparations may have different seeding thresholds, and indicating that micromolar concentrations of tau might not always be required to induce seeding *in vivo*.

Our results have further implications for reporter cell lines, which are widely used for the detection of seed-competent tau assemblies [4, 26, 37]. These systems are optimised for the sensitive detection of seeds by using high expression levels of truncated or mutant tau, transfection reagents to deliver seeds into the cytosol and sensitive microscopy or FACS-based detection. Our results suggest that the dose–response of tau assemblies in a reporter line closely resembles one-hit dynamics. This is beneficial in the sense that the concentration of tau seeds in a sample can be determined irrespective of the dose applied. Indeed, the absence of seeding at low dose in neural settings implies that reporter cell lines may be necessary for detection of seeding activity in many samples. Conversely, our results suggest that caution must be applied when interpreting any seeding detected in these systems, since the absence of one-hit dynamics in neural tissue means that concentrations of tau assemblies that are active in reporter lines may have no activity in a more physiological setting.

#### Evidence of CA1 vulnerability

Our experiments demonstrated that neurons in CA1 were particularly sensitive to seeded aggregation compared to those in CA2 and CA3. Whilst injection of tau assemblies to the *in vivo* brain also demonstrates prominent CA1 seeding, proximity to the injection site is the major determinant of seeding in animal studies, thereby confounding conclusions of regional susceptibility [3, 5, 38]. We found that tau substrate levels were not implicated in the phenotype, suggesting that other factors are responsible for the increased susceptibility. These results are potentially of interest in the study of selective vulnerability since it is well established that CA1 displays more pronounced AT8 reactivity in post-mortem human brains [9, 39, 40]. In humans, the advanced pathology in CA1 versus other HC regions could potentially be

explained either by selective vulnerability of its neurons to aggregation, or by its upstream position in the circuitry of the HC, making it prone to earlier and more pronounced pathology under a spreading model. Our findings lend support to an underlying increased susceptibility of CA1 neurons to pathology. OHSCs therefore provide a suitable platform for future studies to determine the biological basis of this susceptibility.

#### Conclusion

Our findings help define the prion-like characteristics of tau assemblies. Whilst intrinsic seeding activity of recombinant tau assemblies that titrate according to a one-hit dose–response can be detected in biosensor assays, this behaviour is lost in neural tissue. Our findings suggest that neural tissue possesses as yet unidentified homeostatic mechanisms that are capable of successfully preventing seeded aggregation. High levels of tau assemblies are required to overcome these barriers to initiate seeded aggregation.

#### Materials and methods

##### Mouse lines

All animal work was licensed under the UK Animals (Scientific Procedures) Act 1986 and approved by the Medical Research Council Animal Welfare and Ethical Review Body. P301S tau transgenic mice [22] that had been extensively backcrossed to C57BL/6 background were obtained from Dr Michel Goedert, MRC Laboratory of Molecular Biology, UK. Wildtype mice in this study refer to C57BL/6 mice. Male and female mice were used in the study and humanely sacrificed by cervical dislocation.

##### Recombinant tau production

The expression and purification of recombinant human 0N4R tau bearing the P301S mutation from *E. coli* BL-21 (DE3, Agilent Technologies) was performed as described previously (Goedert and Jakes, 1990) with small modifications. Bacterial pellets were collected through centrifugation (3300 g, 4 °C, 10 min) and then resuspended in 10 ml/L of culture with buffer A (50 mM MES pH 6.5, 10 mM EDTA, 14 mM  $\beta$ -mercaptoethanol, 0.1 mM PMSF, 1 mM benzamidine, 1  $\times$  complete EDTA-free protease inhibitors). The resuspended bacteria were lysed on ice using a probe sonicator (approximately 60% amplitude) and then boiled for 10 min at 95 °C to pellet the majority of proteins, while tau will remain in solution as a natively unfolded protein. Denatured proteins were pelleted through ultracentrifugation (100,000 g, 4 °C, 50 min). The clarified supernatant containing monomeric tau P301S was then passed through a HiTrap CaptoS

(Cytiva) cation exchange column and the bound proteins were eluted through a 0–50% gradient elution with Buffer A containing 1 M NaCl. Eluted fractions were assessed through SDS-PAGE and total protein staining with Coomassie InstantBlue. Fractions of interest were concentrated using 10 kDa cut-off Amicon Ultra-4 concentrators (Merck Millipore) before loading on a Superdex 200 10/300 GL (Cytiva) size exclusion chromatography column. The final tau P301S protein was stored in PBS containing 1 mM DTT. All the affinity purification and size exclusion chromatography steps were performed using the ÄKTA Pure system (Cytiva).

#### Recombinant tau aggregation

Tau monomer was added to aggregation buffer (20  $\mu$ M Heparin, 60  $\mu$ M P301S tau monomer, 1  $\times$  complete EDTA-free protease inhibitors, 2  $\mu$ M DTT in PBS) and incubated at 37 °C for 3 days. The resulting P301S tau filaments were sonicated for 15 s before long-term storage at –80 °C.

#### ThioflavinT assay

Tau monomer was added to aggregation buffer, with 10  $\mu$ M sterile filtered ThioflavinT (ThT). Samples were loaded in triplicate into black 96-well plates. Plates were loaded into a CLARIOstar (BMG Labtech), and measurements were taken every 5 min after shaking, for 72 h at 37 °C min (excitation and emission wavelength 440 nm and 510 nm respectively).

#### TEM

Recombinant tau fibrils were mounted on carbon-coated copper grids (EM Resolutions) via suspension of the grid on a single droplet. The grid was then stained with 1% uranyl acetate and imaged with a FEI Tecnai G20 electron microscope operating at 200 kV and an AMT camera.

#### Preparation of tau assemblies from brains and OHSCs

Tau was extracted from aged brains (26 weeks) from mice transgenic for human P301S tau using sarkosyl extraction. Tissues were homogenised for 30 s in 4 volumes of ice-cold H-Buffer (10 mM Tris pH 7.4, 1 mM EGTA, 0.8 M NaCl, 10% sucrose, protease and phosphatase inhibitors (Halt<sup>TM</sup> Protease and Phosphatase Inhibitor Cocktail) using the VelociRuptor V2 Microtube Homogeniser (Scientific Laboratory Supplies). The homogenates were spun for 20 min at 20,000 $\times$ g and supernatant was collected. The resulting pellet was re-homogenised as above in 2 volumes of ice-cold H-Buffer and processed as above. Supernatants from both spins were combined and sarkosyl was added to a final concentration of 1% and incubated for 1 h at 37 °C. Supernatants were then spun at 100,000 $\times$ g at 4 °C for 1 h. The resulting pellet

was resuspended in 0.2 volumes of PBS and sonicated for 15 s in a water-bath sonicator before storage at –80 °C. For OHSCs, the same procedure was followed, except slices were freeze thawed 5 times in 20  $\mu$ l per slice ice-cold H-Buffer and the final pellet was resuspended in 5  $\mu$ l per slice PBS.

#### Western blotting

Samples were transferred to fresh microcentrifuge tubes, to which appropriate volumes of 4 $\times$  NuPAGE LDS sample buffer (Thermo Fisher) containing 50 mM DTT was added and heated to 95 °C for 5 min. Samples were resolved using NuPAGE Bis-Tris Novex 4–12% gels (Life Technologies) and electroblotted to a 0.2- $\mu$ m PVDF membrane using the Transblot Turbo Transfer System (Bio-Rad). Membranes were blocked with 5% milk TBS-Tween 20 before incubation with primary antibodies at 4 °C (Human tau HT7, MN1000, ThermoFisher; CypB, sc-130626, Santa Cruz Biotech; Pan-tau, A0024, DAKO; AT100, MN1060, ThermoFisher; GAPDH-HRP, Proteintech). Membranes were then probed with appropriate secondary antibodies conjugated with HRP for 1 h (Goat anti-mouse-HRP SA00001-1 Proteintech; Goat anti-rabbit-HRP SA00001-2 Proteintech). Membranes were washed repeatedly in TBS–0.1% Tween-20 after both primary and secondary antibody incubation. Blots were incubated with Pierce Super Signal or Millipore Immobilon enhanced chemiluminescence reagents for 5 min and visualised using a ChemiDoc system (Bio-Rad).

#### Dot blot

Recombinant or mouse-extracted tau fibrils were diluted in PBS as indicated in Additional file 1: Supplementary Fig. 1 and applied to 0.2  $\mu$ m nitrocellulose membrane using the Bio-Dot microfiltration apparatus (Bio-Rad). The membranes were then blocked in 5% milk TBS-Tween 20 and subsequently incubated with primary antibody overnight (Pan-tau, A0024, DAKO). The next day, the membranes were probed with goat anti-rabbit secondary antibody conjugated with Alexa488 fluorophore and imaged using the ChemiDoc system (Bio-Rad). The dot intensities were quantified with the Image Studio Lite software (LI-COR Biosciences) and the values for the recombinant fibrils were fitted to a simple linear regression curve.

#### Seeding assay in HEK293

The seeding assay was carried out as described previously [26]. Briefly, HEK293 P301S tau-venus cells were plated at 20,000 cells per well in black 96-well plates pre-coated with poly D-lysine in 50  $\mu$ L OptiMEM (Thermo Fisher). Tau assemblies were diluted in 50  $\mu$ L OptiMEM (Thermo Fisher) and added to cells with 0.5  $\mu$ l per well

Lipofectamine 2000. After 1 h, 100  $\mu$ L complete DMEM was added to each well to stop the transfection process. Cells were incubated at 37 °C in an IncuCyte® S3 Live-Cell Analysis System for 48–72 h after addition of fibrils.

#### Preparation and culturing of organotypic slices

Organotypic hippocampal slice cultures were prepared and cultured according to the protocols described previously [20, 24]. Brains from P6–P9 pups were rapidly removed and kept in ice-cold Slicing Medium (EBSS + 25 mM HEPES) on ice. All equipment was kept ice-cold. Brains were bisected along the midline and the cerebellum was removed using a sterile scalpel. The medial, cut surface of the brain was adhered to the stage of a Leica VT1200S Vibratome using cyanoacrylate (Loctite Super Glue) and the vibratome stage was flooded with ice-cold Slicing Medium. Hemispheres were arranged such that the vibratome blade sliced in a rostral to caudal direction. Sagittal slices of 300  $\mu$ m thickness were prepared and the hippocampus was sub-dissected using sterile needles. Hippocampal slices were transferred to 15 ml tubes filled with ice-cold Slicing Medium using sterile plastic pipettes with the ends cut off. Slices were then transferred onto sterile 0.4  $\mu$ m pore membranes (Millipore PICM0RG50) in 6-well plates pre-filled with 1 ml pre-warmed Culture Medium (50% MEM with GlutaMAX, 18% EBSS, 6% EBSS + D-Glucose, 1% Penicillin–Streptomycin, 0.06% nystatin and 25% Horse Serum) and incubated at 37 °C in a humid atmosphere with 5% CO<sub>2</sub>. Three slices were typically maintained per well. 24 h after plating 100% media was exchanged and thereafter a 50% media exchange was carried out twice per week. For seeding experiments, tau assemblies were diluted in 1 ml Culture Medium and added to the underside of the membrane with 100% media change. After three days, assemblies were removed by 100% media change. Alternatively, 20  $\mu$ l of tau assemblies diluted in Culture Medium was applied directly to OHSCs on the apical side.

#### Adeno-associated virus

AAV1/2.hSyn-GFP particles were generated by co-transfection of HEK293T cells with AAV2/1 (Addgene 112862), AAV2/2 (Addgene 104963), adenovirus helper plasmid pAdDeltaF6 (Addgene 112867) and pAAV-hSyn-EGFP (Addgene 50465). Virus particles were purified by iodixanol gradient in at T70i ultracentrifuge rotor as previous [41]. Viral purity was confirmed by the presence of three bands following SDS-PAGE and staining with Coomassie InstantBlue and viral titre was determined by quantitative PCR.

#### Immunofluorescence microscopy

Slices on membranes were washed with PBS and then fixed in 4% (w/v) paraformaldehyde for 20 min at 37 °C. Subsequently, membranes were rinsed 2–3 times with PBS and left shaking gently for 15 min to remove traces of paraformaldehyde before subsequent processing. Slices were cut from the insert using a scalpel, leaving ample membrane around the circumference of the slice, and placed with tweezers, slice side up, into 24 well plates for staining. Slices were permeabilised with 300  $\mu$ l 0.5% (v/v) Triton X-100 in immunofluorescence blocking buffer (IF block) (3% goat serum in 1  $\times$  PBS) for 1 h at room temperature and rinsed 3 times with TBS. Slices were then incubated with primary antibodies (MAP2, ab5392, Abcam; human tau HT7, MN1000, ThermoFisher; pan-tau, A0024, DAKO; phospho-tau AT8, MN1020 ThermoFisher; Gfap, G3893, Sigma; Iba1, ab178846, Abcam) diluted in IF block overnight at 4 °C, rinsed with 3 times with TBS, and incubated for 2 h in the dark with secondary antibodies, also diluted in IF block. Secondary antibodies conjugated to Alexa Fluor 488, 568 or 647 were obtained from Thermo Fisher. Following rinsing 3 times with TBS, the slices were incubated with Hoechst stain for 10 min and rinsed 3 times with TBS. Membranes were placed on slides (slice side up), mounting medium (ProLong Diamond, Life Technologies) was added and a cover slip was placed on top of the slices. Images were captured using a Zeiss LSM780 Confocal Microscope with either a 20 $\times$  or a 63 $\times$  objective lens. Images were collected and stitched, where appropriate, using ZEISS Zen software package.

#### Image analysis and statistics

For tau seeding assays in HEK293 cells, aggregates were detected and quantified using the ComDet plugin in Fiji [42]. Threshold levels for detection of aggregates were adjusted using mock-seeded images for each experiment. Levels of seeding were calculated as (number of aggregates)/(total cells)  $\times$  100 for individual fields. For slice cultures, maximum intensity Z-projections were interrogated for AT8 immunoreactivity by the application of a binary threshold-based mask in ImageJ. Percent area of AT8 reactivity was determined in regions of 100  $\times$  100  $\mu$ m. GFP positive neurons upon AAV infection were analysed in the same way. For measures of number of neurons affected in hippocampal subregions, a manual count of cell bodies positive for AT8 immunoreactivity was performed. Zero values were given an arbitrary value of 10<sup>-5</sup> for representation on log-scale axes. The data in

all graphs are represented as the mean  $\pm$  SD. Data was analysed via the Kruskal–Wallis test by ranks, unless it was determined to be normally distributed, in which case a one-way ANOVA was employed. All statistics were carried out in GraphPad Prism Version 8.

## Supplementary Information

The online version contains supplementary material available at <https://doi.org/10.1186/s40478-021-01141-6>.

**Additional file 1:** Supplementary Figures.

## Acknowledgements

We thank Dr Michel Goedert for provision of P301S tau transgenic mice and Cambridge Advanced Imaging Centre for access to electron microscope facilities. We thank Prof Sir David Klenerman for valuable discussions on the early versions of this manuscript.

## Authors' contributions

Conceived research: WAM, MPC, ASM, LVCM; Designed experiments: ASM, LVCM, WAM; Developed slice culture assay: ASM, LVCM, CD, OS, BJT, CK, MJV, LCJ; Performed experiments and analysed data: LVCM, ASM, TK, BJT, WAM, SS, SC. All authors contributed to writing and editing of the manuscript.

## Funding

WAM is supported by a Sir Henry Dale Fellowship jointly funded by the Wellcome Trust and the Royal Society (Grant No. 206248/Z/17/Z). This work was supported by the UK Dementia Research Institute which receives its funding from DRI Ltd, funded by the UK Medical Research Council, Alzheimer's Society and Alzheimer's Research UK. This project has received funding from the Innovative Medicines Initiative 2 Joint Undertaking under Grant agreement No. 116060 (IMPRIND). This Joint Undertaking receives support from the European Union's Horizon 2020 research and innovation programme and EFPIA. This work is supported by the Swiss State Secretariat for Education, Research and Innovation (SERI) under contract number 17.00038. The work also received funding from Takeda Pharmaceuticals Company. LVCM is supported by the UK Medical Research Council.

## Declarations

### Competing interests

The authors declare that they have no competing interests.

### Ethics approval

All animal work was licensed under the UK Animals (Scientific Procedures) Act 1986 and approved by the Medical Research Council Animal Welfare and Ethical Review Body.

### Author details

<sup>1</sup> Department of Clinical Neurosciences, UK Dementia Research Institute at the University of Cambridge, Cambridge, UK. <sup>2</sup> John Van Geest Centre for Brain Repair, University of Cambridge, Cambridge, UK. <sup>3</sup> MRC Laboratory of Molecular Biology, Francis Crick Avenue, Cambridge, UK. <sup>4</sup> Centre for Discovery Brain Sciences, University of Edinburgh, Edinburgh, UK.

Received: 6 January 2021 Accepted: 26 February 2021

Published online: 12 March 2021

## References

- Goedert M (2015) Alzheimer's and Parkinson's diseases: The prion concept in relation to assembled A $\beta$ , tau, and  $\alpha$ -synuclein. *Science* 349:1255–1255
- Jucker M, Walker LC (2018) Propagation and spread of pathogenic protein assemblies in neurodegenerative diseases. *Nat Neurosci* 21:1341–1349
- Clavaguera F, Bolmont T, Crowther RA, Abramowski D, Frank S, Probst A et al (2009) Transmission and spreading of tauopathy in transgenic mouse brain. *Nat Cell Biol* 11:909–913
- Frost B, Jacks RL, Diamond MI (2009) Propagation of tau misfolding from the outside to the inside of a cell. *J Biol Chem* 284:12845–12852
- Iba M, Guo JL, McBride JD, Zhang B, Trojanowski JQ, Lee VM-Y (2013) Synthetic tau fibrils mediate transmission of neurofibrillary tangles in a transgenic mouse model of Alzheimer's-like tauopathy. *J Neurosci Soc Neurosci* 33:1024
- Narasimhan S, Guo JL, Changolkar L, Stieber A, McBride JD, Silva LV et al (2017) Pathological tau strains from human brains recapitulate the diversity of tauopathies in nontransgenic mouse brain. *J Neurosci Off J Soc Neurosci* 37:11406–11423
- Goedert M, Jakes R, Vanmechelen E (1995) Monoclonal antibody AT8 recognises tau protein phosphorylated at both serine 202 and threonine 205. *Neurosci Lett* 189:167–170
- Braak H, Thal DR, Ghebremedhin E, Del Tredici K (2011) Stages of the pathologic process in Alzheimer disease: age categories from 1 to 100 years. *J Neuropathol Exp Neurol* 70:960–969
- Braak H, Braak E (1991) Neuropathological staging of Alzheimer-related changes. *Acta Neuropathol (Berl)* 82:239–259
- Nelson PT, Alafuzoff I, Bigio EH, Bouras C, Braak H, Cairns NJ et al (2012) Correlation of Alzheimer disease neuropathologic changes with cognitive status: a review of the literature. *J Neuropathol Exp Neurol* 71:362–381
- Yamada K, Cirrito JR, Stewart FR, Jiang H, Finn MB, Holmes BB et al (2011) In vivo microdialysis reveals age-dependent decrease of brain interstitial fluid tau levels in P301S human tau transgenic mice. *J Neurosci* 31:13110–13117
- Sjögren M, Vanderstichele H, Agren H, Zachrisson O, Edsbacke M, Wikkelso C et al (2001) Tau and Abeta42 in cerebrospinal fluid from healthy adults 21–93 years of age: establishment of reference values. *Clin Chem* 47:1776–1781
- Blennow K (2017) A review of fluid biomarkers for Alzheimer's disease: moving from CSF to blood. *Neurol Ther* 6:15–24
- Dulbecco R, Vogt M (1953) Some problems of animal virology as studied by the plaque technique. *Cold Spring Harb Symp Quant Biol* 18:273–279
- Masel J, Jansen VAA (2001) The measured level of prion infectivity varies in a predictable way according to the aggregation state of the infectious agent. *Biochim Biophys Acta BBA Mol Basis Dis* 1535:164–173
- Dunwiddie T, Lynch G (1978) Long-term potentiation and depression of synaptic responses in the rat hippocampus: localization and frequency dependency. *J Physiol* 276:353–367
- Cho S, Wood A, Bowlby MR (2007) Brain slices as models for neurodegenerative disease and screening platforms to identify novel therapeutics. *Curr Neuropharmacol* 5:19–33
- Croft CL, Futch HS, Moore BD, Golde TE (2019) Organotypic brain slice cultures to model neurodegenerative proteinopathies. *Mol Neurodegener* 14:45
- Duff K, Noble W, Gaynor K, Matsuoka Y (2002) Organotypic slice cultures from transgenic mice as disease model systems. *J Mol Neurosci* 19:317–320
- Harwell CS, Coleman MP (2016) Synaptophysin depletion and intraneuronal A $\beta$  in organotypic hippocampal slice cultures from huAPP transgenic mice. *Mol Neurodegener* 11:44
- Croft CL, Wade MA, Kurbatskaya K, Mastrandreas P, Hughes MM, Phillips EC et al (2017) Membrane association and release of wild-type and pathological tau from organotypic brain slice cultures. *Cell Death Dis* 8:e2671
- Allen B, Ingram E, Takao M, Smith MJ, Jakes R, Virdee K et al (2002) Abundant tau filaments and nonapoptotic neurodegeneration in transgenic mice expressing human P301S tau protein. *J Neurosci Off J Soc Neurosci* 22:9340–9351
- Kundel F, Hong L, Falcon B, McEwan WA, Michaels TCT, Meisl G et al (2018) Measurement of tau filament fragmentation provides insights into prion-like spreading. *ACS Chem Neurosci* 9:1276–1282
- De Simoni A, Lily MY (2006) Preparation of organotypic hippocampal slice cultures: interface method. *Nat Protoc* 1:1439–1445
- Sheppard O, Coleman MP, Durrant CS (2019) Lipopolysaccharide-induced neuroinflammation induces presynaptic disruption through a direct



- action on brain tissue involving microglia-derived interleukin 1 beta. *J Neuroinflamm* 16:106
26. McEwan WA, Falcon B, Vaysburd M, Clift D, Oblak AL, Ghetti B et al (2017) Cytosolic Fc receptor TRIM21 inhibits seeded tau aggregation. *Proc Natl Acad Sci U S A* 114:574–579
  27. Takeda S, Commins C, DeVos SL, Nobuhara CK, Wegmann S, Roe AD et al (2016) Seed-competent high-molecular-weight tau species accumulates in the cerebrospinal fluid of Alzheimer's disease mouse model and human patients. *Ann Neurol* 80:355–367
  28. Saijo E, Ghetti B, Zanusso G, Oblak A, Furman JL, Diamond MI et al (2017) Ultrasensitive and selective detection of 3-repeat tau seeding activity in Pick disease brain and cerebrospinal fluid. *Acta Neuropathol (Berl)* 133:751–765
  29. Saijo E, Metrick MA, Koga S, Parchi P, Litvan I, Spina S et al (2020) 4-Repeat tau seeds and templating subtypes as brain and CSF biomarkers of frontotemporal lobar degeneration. *Acta Neuropathol (Berl)* 139:63–77
  30. Shi J, Aiken C (2006) Saturation of TRIM5 $\alpha$ -mediated restriction of HIV-1 infection depends on the stability of the incoming viral capsid. *Virology* 350:493–500
  31. Hatzioannou T, Cowan S, Goff SP, Bieniasz PD, Towers GJ (2003) Restriction of multiple divergent retroviruses by Lv1 and Ref1. *EMBO J* 22:385–394
  32. Zhang W, Falcon B, Murzin AG, Fan J, Crowther RA, Goedert M et al (2019) Heparin-induced tau filaments are polymorphic and differ from those in Alzheimer's and Pick's diseases. *eLife* 8:e43584
  33. Ando K, Leroy K, Héraud C, Yilmaz Z, Authélet M, Suain V et al (2011) Accelerated human mutant tau aggregation by knocking out murine tau in a transgenic mouse model. *Am J Pathol* 178:803–816
  34. Wang Y, Balaji V, Kaniyappan S, Krüger L, Irsen S, Tepper K et al (2017) The release and trans-synaptic transmission of Tau via exosomes. *Mol Neurodegener* 12:5
  35. Tardivel M, Bégard S, Bousset L, Dujardin S, Coens A, Melki R et al (2016) Tunneling nanotube (TNT)-mediated neuron-to neuron transfer of pathological Tau protein assemblies. *Acta Neuropathol Commun BioMed Central* 4:1–14
  36. Skachokova Z, Martinisi A, Flach M, Sprenger F, Naegelin Y, Steiner-Monard V et al (2019) Cerebrospinal fluid from Alzheimer's disease patients promotes tau aggregation in transgenic mice. *Acta Neuropathol Commun* 7:72
  37. Woerman AL, Aoyagi A, Patel S, Kazmi SA, Lobach I, Grinberg LT et al (2016) Tau prions from Alzheimer's disease and chronic traumatic encephalopathy patients propagate in cultured cells. *Proc Natl Acad Sci* 113:E8187–E8196
  38. Ahmed Z, Cooper J, Murray TK, Garn K, McNaughton E, Clarke H et al (2014) A novel in vivo model of tau propagation with rapid and progressive neurofibrillary tangle pathology: the pattern of spread is determined by connectivity, not proximity. *Acta Neuropathol (Berl)* 127:667–683
  39. Furcila D, Domínguez-Álvaro M, DeFelipe J, Alonso-Nanclares L (2019) Subregional density of neurons, neurofibrillary tangles and amyloid plaques in the hippocampus of patients with Alzheimer's disease. *Front Neuroanat*. <https://doi.org/10.3389/fnana.2019.00099/full>
  40. Lace G, Savva GM, Forster G, de Silva R, Brayne C, Matthews FE et al (2009) Hippocampal tau pathology is related to neuroanatomical connections: an ageing population-based study. *Brain* 132:1324–1334
  41. Zolotukhin S, Byrne BJ, Mason E, Zolotukhin I, Potter M, Chesnut K et al (1999) Recombinant adeno-associated virus purification using novel methods improves infectious titer and yield. *Gene Ther* 6:973–985
  42. Schindelin J, Arganda-Carreras I, Frise E, Kaynig V, Longair M, Pietzsch T et al (2012) Fiji: an open-source platform for biological-image analysis. *Nat Methods* 9:676–682

### Publisher's Note

Springer Nature remains neutral with regard to jurisdictional claims in published maps and institutional affiliations.

Ready to submit your research? Choose BMC and benefit from:

- fast, convenient online submission
- thorough peer review by experienced researchers in your field
- rapid publication on acceptance
- support for research data, including large and complex data types
- gold Open Access which fosters wider collaboration and increased citations
- maximum visibility for your research: over 100M website views per year

At BMC, research is always in progress.

Learn more [biomedcentral.com/submissions](https://biomedcentral.com/submissions)

